
















SN 2023zaw: the low-energy explosion of an ultra-stripped star, with non-radioactive heating

T. MOORE ^{1,2} J. H. GILLANDERS ³ M. NICHOLL ¹ M. E. HUBER,⁴ S. J. SMARTT ^{3,1} S. SRIVASTAV ³
H. F. STEVANCE,^{3,1,5} T.-W. CHEN ⁶ K. C. CHAMBERS,⁴ J. P. ANDERSON ^{2,7} M. D. FULTON ¹ S. R. OATES ⁸
C. ANGUS,¹ G. PIGNATA,⁹ N. ERASMUS ¹⁰ H. GAO ⁴ J. HERMAN,⁴ C.-C. LIN,⁴ T. LOWE,¹¹ E. A. MAGNIER ¹¹
P. MINGUEZ,¹¹ C.-C. NGEOW ⁶ X. SHENG,¹ S. A. SIM ¹ K. W. SMITH,¹ R. WAINSCOT,¹¹ S. YANG,¹²
D. R. YOUNG ¹ AND K.-J. ZENG⁶

¹*Astrophysics Research Centre, School of Mathematics and Physics, Queen's University Belfast, BT7 1NN, UK*

²*European Southern Observatory, Alonso de Córdova 3107, Casilla 19, Santiago, Chile*

³*Astrophysics sub-Department, Department of Physics, University of Oxford, Keble Road, Oxford, OX1 3RH, UK*

⁴*Institute for Astronomy, University of Hawai'i, 2680 Woodlawn Drive, Honolulu, HI 96822, USA*

⁵*Department of Physics, The University of Auckland, Private Bag 92019, Auckland, New Zealand*

⁶*Graduate Institute of Astronomy, National Central University, 300 Jhongda Road, 32001 Jhongli, Taiwan*

⁷*Millennium Institute of Astrophysics (MAS), Nuncio Monseñor Sótero Sanz 100, Providencia, Santiago, Chile*

⁸*Department of Physics, Lancaster University, Lancaster, LA1 4YB, UK*

⁹*Instituto de Alta Investigación, Universidad de Tarapacá, Arica, Casilla 7D, Chile*

¹⁰*South African Astronomical Observatory, PO Box 9, Observatory 7935, Cape Town, South Africa*

¹¹*Institute for Astronomy, University of Hawaii, 2680 Woodlawn Drive, Honolulu, HI 96822*

¹²*Henan Academy of Sciences, Zhengzhou 450046, Henan, China*

ABSTRACT

Most stripped envelope supernova progenitors are formed through binary interaction, losing hydrogen and/or helium from their outer layers. An emerging class of supernovae with the highest degree of envelope-stripping are thought to be the product of stripping by a NS companion. However, relatively few examples are known and the outcomes of such systems can be diverse and are poorly understood at present. Here, we present spectroscopic observations and high cadence multi-band photometry of SN 2023zaw, a low ejecta mass and rapidly evolving supernova. SN 2023zaw was discovered in a nearby spiral galaxy at $D = 39.7$ Mpc, with significant Milky Way extinction, $E(B - V) = 0.21$, and significant (but uncertain) host extinction. Bayesian evidence comparison reveals that nickel is not the only power source and an additional energy source is required to explain our observations. Our models suggest an ejecta mass of $M_{\text{ej}} \sim 0.07 M_{\odot}$ and a synthesised nickel mass of $M_{\text{ej}} \sim 0.007 M_{\odot}$ is required to explain the explosion. However an additional heating from a magnetar or interaction with circumstellar material is required to power the early light curve.

Keywords: Transient sources (1851) — Supernovae (1668) — Core-collapse supernovae (304) – Type Ib supernovae (1729) – Circumstellar matter (241)

1. INTRODUCTION

Modern sky surveys such as the Asteroid Terrestrial-impact Last Alert System (ATLAS; Tonry et al. 2018), Zwicky Transient Facility (ZTF; Bellm et al. 2019), and the Panoramic Survey Telescope and Rapid Response System (Pan-STARRS; Chambers et al. 2016) are re-

vealing the extremes of core-collapse supernovae (SNe) and optical transients (Inserra 2019; Modjaz et al. 2019). A small number of SNe, often belonging to the hydrogen poor Types Ib and Ic, show rapid evolution and brighten and fade on timescales much faster than typical classes of SNe (Poznanski et al. 2010; Drout et al. 2013; De et al. 2018; Prentice et al. 2018, 2020; Chen et al. 2020; Yan et al. 2023; Ho et al. 2023). Generally, a small ejecta mass is invoked to explain the rapid evolution of fast transients (Moriya et al. 2017). A small ejecta mass reduces the photon diffusion timescale allowing the

light curve to peak and begin to decline rapidly. Low ejecta mass interpretations require a physically compatible powering source. Invoking radioactive ^{56}Ni in fast evolving SNe frequently produces unphysical ejecta mass to nickel mass ratios (Prentice et al. 2018; Gillanders et al. 2020; Prentice et al. 2020; Chen et al. 2020). Additional mechanisms have been suggested to boost the luminosity of these supernovae e.g circumstellar material interaction, energy injection from a magnetar, and shock cooling emission (Yao et al. 2020; Sawada et al. 2022)

In this paper, we present spectrophotometric follow-up observations of the rapidly evolving SN 2023zaw.¹ We determine a time of maximum light of MJD 60287.1 ± 0.2 from fitting a polynomial to the ZTF g -band. Classified as a Type Ib, SN 2023zaw rises rapidly to maximum light (< 4 days) followed by a similarly fast decline, comparable to the fastest fading Type I SN 2019bk (Chen et al. 2020; Prentice et al. 2020).

2. DISCOVERY AND FOLLOW-UP

SN 2023zaw was discovered on 2023 December 7 05:34 UT (MJD 60285.23) by ZTF (Bellm et al. 2019) and registered on the Transient Name Server at 11:50 UT (Sollerman 2023) with the discovery mag $g = 19.34$. We independently detected SN 2023zaw in ATLAS data (Smith et al. 2020) a few hours later at 08:00 UT as the field visibility moved from California to Hawaii, at mag $o = 18.74$. The transient is offset $8.97''$ N, $19.15''$ W from UGC 03048, a spiral galaxy with a redshift from the NASA Extragalactic Database (NED) of 0.010150 ± 0.000026 (Springob et al. 2005). From NED the median redshift-independent distance to UGC 03048 is 39.7 Mpc, based on the Tully-Fisher method (Tully et al. 2013). The SN is offset $8.97''$ North and $19.15''$ West, or 4.1 kpc, from the galaxy center. SN 2023zaw is located on the edge of one of the two prominent arms of UGC 03048. The Milky Way extinction along this line of sight is $A_V = 0.6555$ mag (Schlafly & Finkbeiner 2011). Na I D lines in the classification spectrum suggest additional host extinction is significant (Poznanski et al. 2012).

Four AstroNotes regarding SN 2023zaw were released on the Transient Name Server² at the time of discovery, commenting on its early evolution. Karambelkar et al. (2023a) highlighted the discovery and fast fading nature of SN 2023zaw, along with an observation of the transient with NOT/ALFOSC. The Kinder project (Lee et al. 2023) reported a color-dependent fade us-

ing observations performed on the 40-cm SLT at Lulin Observatory, Taiwan. In Fulton et al. (2023), we reported the combined ATLAS and ZTF data and highlighted that this source was flagged by our ‘Fastfinder’ filter and annotator on the Lasair broker³ (Smith et al. 2019) to find fast evolving objects in the ZTF public alert stream. Both Karambelkar et al. (2023a) and Fulton et al. (2023) identified SN 2023zaw as a fast-fading, sub-luminous and red transient. Spectroscopic observations with Keck (Karambelkar et al. 2023b) reported an apparent similarity with the candidate ‘Ia’ SN 2010X (Kasliwal et al. 2010). Finally, Gillanders et al. (2023) classified the object as a Type Ib SN based on observations performed with Gemini-N/GMOS, and this spectrum was immediately made public on the TNS.

2.1. Photometry

Photometry for SN 2023zaw (internal name ATLAS23wuw) were obtained from the ATLAS forced photometry server (Shingles et al. 2021) and binned by day. The ATLAS (Tonry et al. 2018) system is a all-sky survey for potentially dangerous near-Earth objects. ATLAS data are processed using the ATLAS Science Server (Smith et al. 2020) to search for stationary transients. We obtained measurements in the g and r -bands using the Lasair broker (Smith et al. 2019) and public ZTF stream data⁴.

We triggered follow-up observations with the 1.8m Pan-STARRS1 on the Haleakala mountain, Hawaii (Chambers et al. 2016). The Pan-STARRS1 telescope has a 7 deg^2 field of view and features a 1.4 gigapixel camera. Observations in the $grizy_{P1}$ were taken with a daily cadence between MJD 60291 and 60295. An additional riz_{P1} epoch was taken on MJD 60302, all further Pan-STARRS observations were performed using the iz_{P1} bands. Optical imaging was triggered with the 2.0-m Liverpool Telescope (LT; Steele et al. 2004) using IO:O in riz bands under program PL23B26 (PI: M. Fulton). Measurements were made by PSF fitting using Source-Extractor (Bertin & Arnouts 1996) without host-galaxy subtraction. We observed SN 2023zaw with the 0.4m SLT telescope as a part of the Kinder project (Chen et al. 2021) and measured psf $griz$ -band photometry. Three epochs of photometric observations were performed with the GMOS-N instrument at the Gemini-North 8.1-m telescope, under program ID GN-2023B-Q-125 (PI: M. Huber). These were obtained at MJDs 60329.2 (riz -band), 60339.3 (riz -band) and 60341.2 (ri -band). These observations were

¹ While preparing this manuscript, another pre-print on the same source appeared on the arXiv (Das et al. 2024).

² <https://www.wis-tns.org/object/2023zaw>

³ <https://lasair-ztf.lsst.ac.uk>

⁴ <https://lasair-ztf.lsst.ac.uk/objects/ZTF23absbqun>

bias-subtracted and flat-field corrected using standard recipes in DRAGONS (Labrie et al. 2023; Labrie et al. 2023). We also present three epochs of r -band photometry derived from the acquisition images obtained prior to our spectroscopic observations with GMOS-N (see Section 2.2 for details). Aperture photometry was performed using PSF (Nicholl et al. 2023) with a small optimised aperture, an encircled energy correction, and local background subtraction.

The Ultra-Violet and Optical Telescope (UVOT; Roming et al. 2005) onboard the *Neil Gehrels Swift Observatory* (Swift; Gehrels et al. 2004) satellite observed SN 2023zaw on MJD 60293 and MJD 60296. A single *uvm2* exposure was performed on MJD 60291. While observations were taken in the u , b , v , *uvw1*, *uvm2* and *uvw2* bands on days MJD 60293 and MJD 60296. The images at each epoch were co-added, and the count rates obtained from the stacked images using the *Swift* tool *uvotsource*. To extract the source counts, we used a source aperture of $5''$ radius and an aperture of $20''$ radius for the background. The source count rates were converted to magnitudes using the UVOT photometric zero points (Poole et al. 2008; Breeveld et al. 2011). All *Swift* observations are non-detections of the transient.

The Milky Way extinction-corrected light curve of SN 2023zaw is presented in Figure 1. All photometry will be provided in the online version of this paper and as a machine readable table.

2.2. Spectroscopy

We observed SN 2023zaw at three different phases with the Gemini-North/GMOS-N instrument under program ID GN-2023B-Q-125 (PI: M. Huber). Our three observations commenced on MJDs 60291.3, 60295.3 and 60313.4 (corresponding to phases from maximum light of $\approx +4.2$, $+8.2$ and $+26.0$ days, respectively). All observations were performed using the R400 grating, sampling the $\approx 4200\text{--}9100\text{ \AA}$ wavelength range at a spectral resolution of $R \sim 2000$.

We reduced all three epochs of Gemini observations using the DRAGONS pipeline (Labrie et al. 2023; Labrie et al. 2023) following standard recipes, and the spectra were all flux-calibrated against the same standard star. The contribution of the host galaxy was estimated and subtracted, and each reduced, co-added spectrum agrees well with the background-subtracted Pan-STARRS photometry obtained at the same epoch. All spectra in this work will be made publicly available on the WISerEP repository (Yaron & Gal-Yam 2012).

3. ANALYSIS

3.1. Host Galaxy and Milky Way Foreground Extinction

There is a strong and narrow absorption line in the $+4.2$ and $+8.2$ day GMOS-N spectra, consistent with Na I D absorption at the redshift of UGC 03048. The GMOS-N spectral resolution does not allow the D_1 and D_2 components to be separately measured. After normalising the spectrum, we fit a single Gaussian to the blended absorption line, with a centre $\lambda_c = 5953.94\text{ \AA}$ ($z = 0.0104$), a FWHM width = 11.4 \AA , and an equivalent width, $EW = 2.10 \pm 0.22\text{ \AA}$.

Measurements of the equivalent width of the Na I doublet have been shown to be correlated with the line-of-sight extinction (Poznanski et al. 2012), and this method has often been applied to extragalactic transients. While there is a reasonably linear relation between line strength and $E(B - V)$, up to a total $EW_{(D_1+D_2)} \simeq 0.7\text{ \AA}$, the relationship then saturates. No quantitative and unique measurement of $E(B - V)$ appears possible beyond this, but we can say that an $EW = 2.10 \pm 0.22\text{ \AA}$ requires a minimum of $E(B - V)_{\text{host}} \gtrsim 0.5$. The Milky Way foreground extinction is also significant along this line of sight, with $E(B - V)_{\text{MW}} = 0.2$ (Schlafly & Finkbeiner 2011). Throughout the rest of this manuscript, we apply a total extinction of $E(B - V) = 0.7$, noting that a somewhat higher value cannot be discounted.

3.2. Light Curves

The light curves of SN 2023zaw are shown in Figure 1. Shortly after discovery, SN 2023zaw reaches a maximum brightness of $r = 17.6$ mag and $g = 18$ mag. The rapid rising phase of the light curve is not well observed, but the time from explosion to g -band peak is constrained to be less than four days by the ATLAS o -band non-detections (at depths correspond to M_o of -14.5 and -14.8 mag) at 2.7 and 1.8 days pre-discovery, respectively. The photometric evolution after maximum light is similarly rapid. Due to the short rise time we only observe the rising portion of the light curve in the go -bands. SN 2023zaw evolves extremely fast when compared to the representative Type Ib SN 2007Y (Stritzinger et al. 2009) in Figure 2. Initially SN 2023zaw fades ~ 3 magnitudes in ~ 10 days in the r -band, with SN 2007Y fading by less than a magnitude during the same interval. After this early rapid fade, SN 2023zaw is comparable to SN 2019bkc which is the fastest known Type I SN. SN 2023zaw settles to an apparent radioactive tail which we observe in the riz -bands.

3.3. Light Curve Modeling

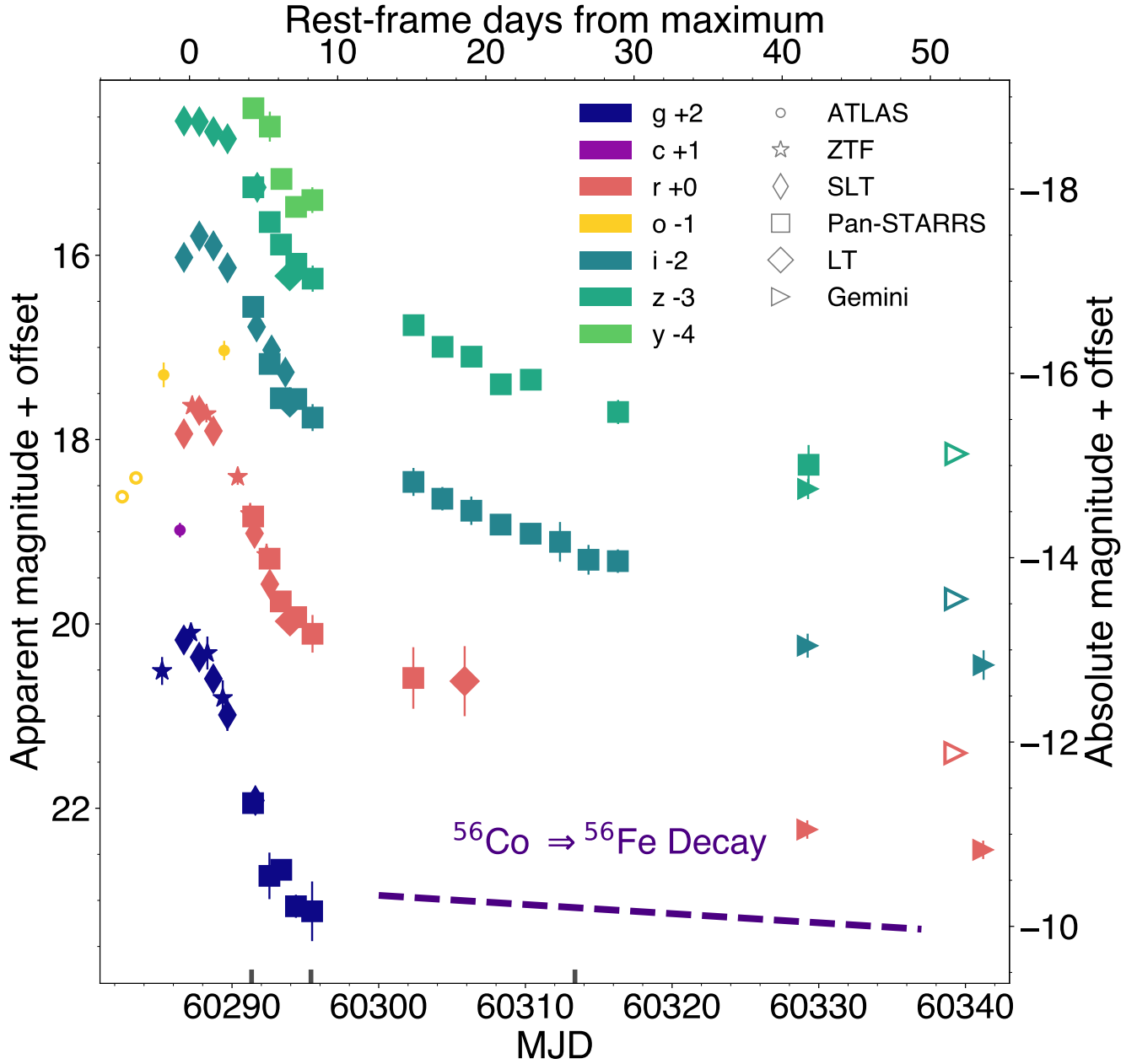


Figure 1. Multicolor light curves with corrections for Milky Way foreground extinction and time dilation for ($z = 0.010150$) applied. Each telescope is shown with a different marker and unfilled markers indicate upper limits. We exclude *Swift*/UVOT non-detections for visual clarity. Additionally we show the expected decline rate of a ^{56}Co tail ($0.98 \text{ mag} / 100 \text{ day}$) (Woosley et al. 1989).

We use the Modular Open Source Fitter for Transients MOSFiT⁵ which is a Python-based modular code which evaluates a user-defined physical model to the observed light curves of transients. The code is described in detail by Guillochon et al. (2018). We use the *dynesty* (Spea-

gle 2020) nested sampling package option in MOSFiT to evaluate for a series of different models. For all models we assume an optical opacity (κ) of $0.1 \text{ cm}^2 \text{ g}^{-1}$ and a gamma-ray opacity (κ_γ) of $0.027 \text{ cm}^2 \text{ g}^{-1}$. We apply a constraint to the host galaxy H column density of $n_{\text{H,host}}(\text{cm}^{-2}) > 3.43 \times 10^{21}$ for consistency with our adopted minimum host extinction (Section 3.1), assuming $R_V = 3.1$ and $n_{\text{H}}(\text{cm}^{-2})/A_V = 2.21 \times 10^{21}$ (Güver &

⁵ <https://github.com/guillochon/MOSFiT>

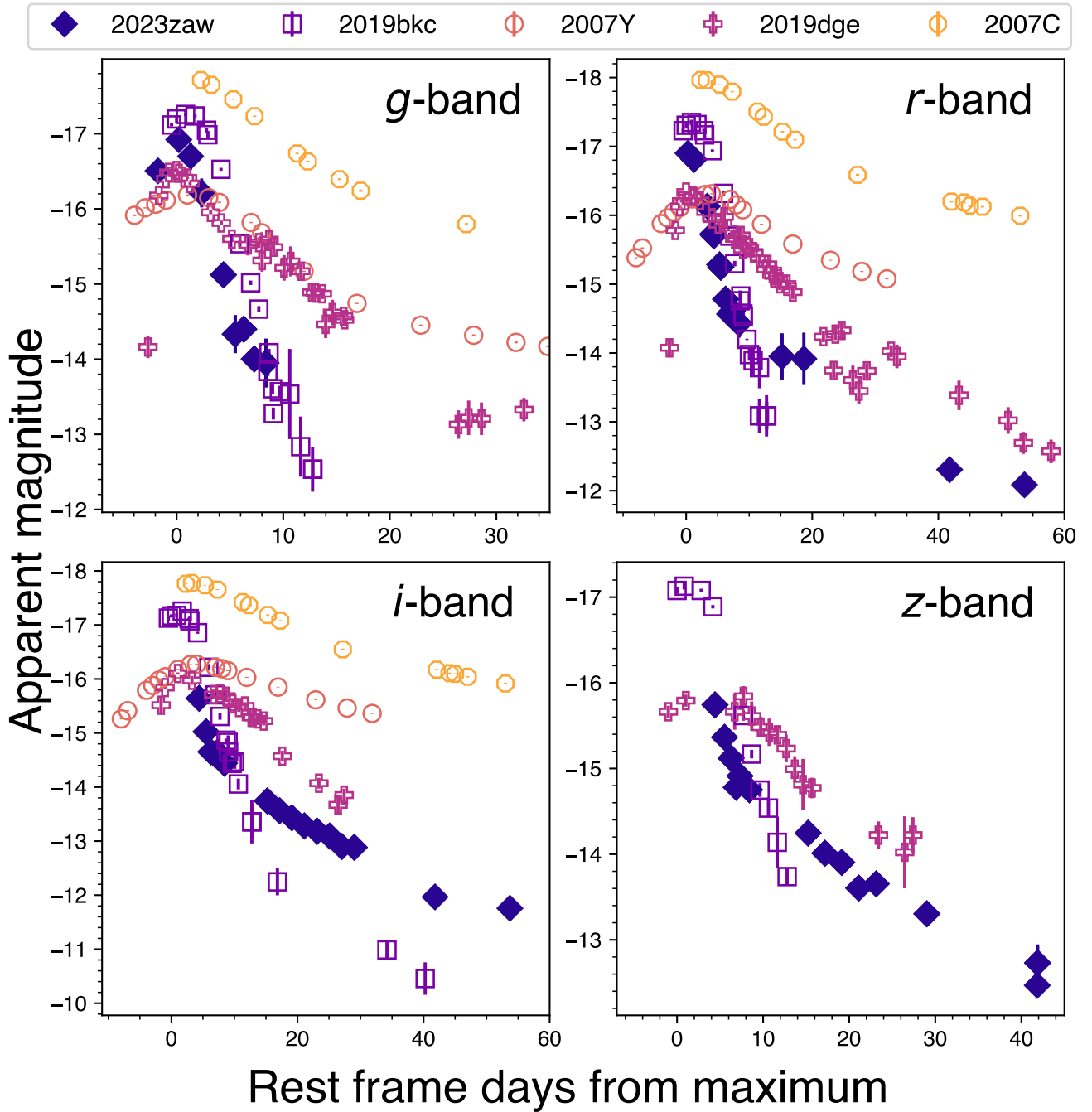


Figure 2. Light curves of SN 2023zaw in the *griz*-bands compared to the fast supernovae SN 2019bkc (Prentice et al. 2020; Chen et al. 2020), SN 2019dge (Yao et al. 2020), and the representative Type SN Ib SNe 2007Y (Stritzinger et al. 2009) and SN 2007C (Drout et al. 2011; Stritzinger et al. 2018). Each light curve is in the rest frame and has been corrected for Milky Way and host galaxy extinctions (Drout et al. 2011). These supernovae were chosen to represent the population USSNe and typical Type Ib SNe.

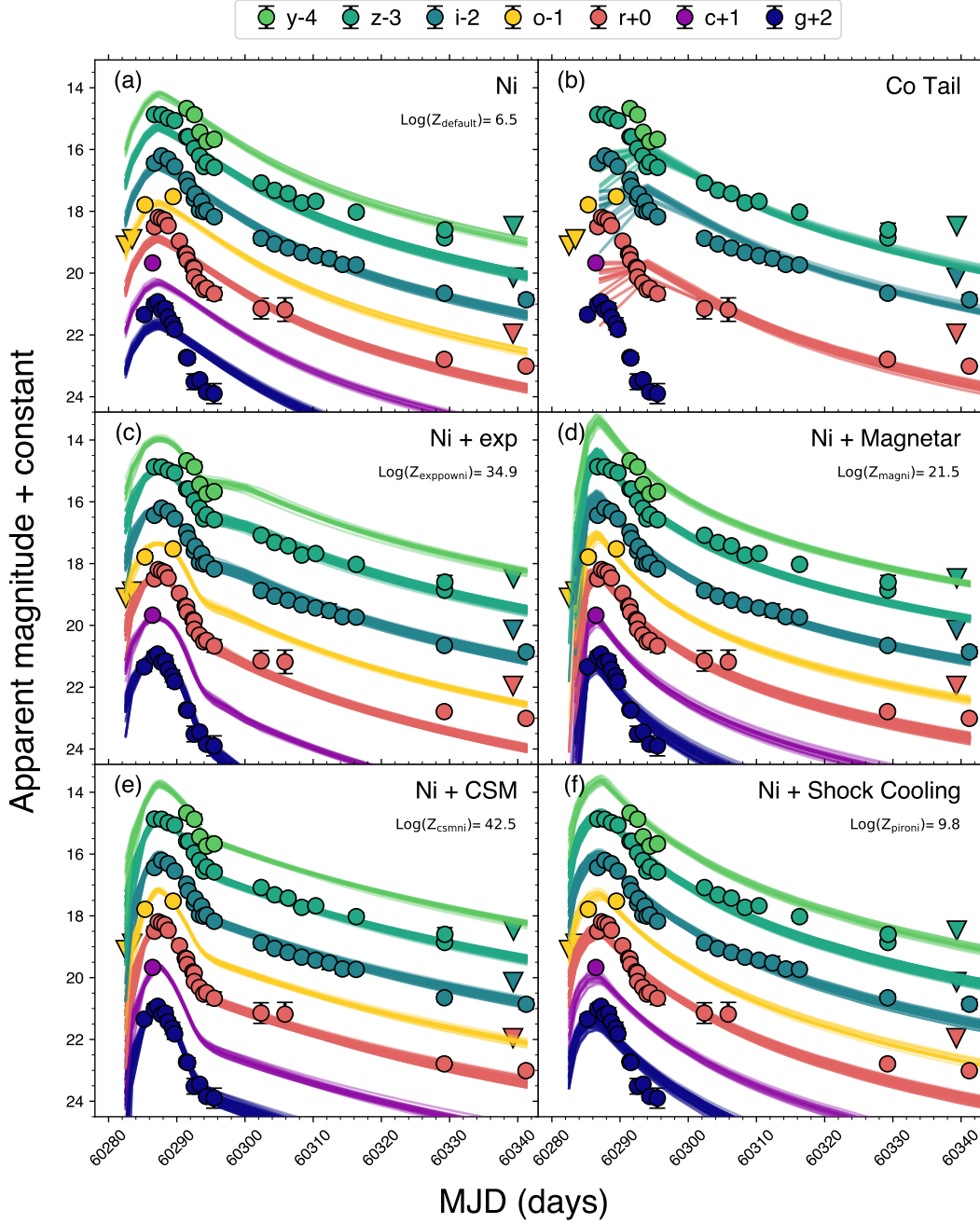


Figure 3. Fit results to the complete light curves using MOSFiT (Guillochon et al. 2018) for our physical models compared to photometry, where downward arrows are upper-limits, realisations are repeated as solid lines and, band colors match those in Figure 1. Panel (a) shows nickel-only model realisations. Panels (c), (d), and (e) show the nickel + exp model, magnetar + nickel model, and circumstellar material interaction + Nickel models respectively. Panel (b) shows a fit to only the late-time light curve to estimate a synthesized nickel-mass, and Panel (f) shows our shock-cooling emission + nickel, the shock cooling model follows (Piro et al. 2021). The Bayesian evidence for each model is calculated for model comparison. When quoting the evidence for each model the name of each model in the MOSFiT code is used to ensure the reproducibility of these results. Model evidence is not included in panel (b) as the model is only evaluated against the light curve tail. The MOSFiT input file will be made available as a data behind the figure file with the online article and all models are or will be made publicly available

Özel 2009). All models that are considered in this work are shown in Figure 3 together with the observed light curves of SN 2023zaw.

The rising phase of SN 2023zaw is poorly sampled compared to the peak and tail of the light curve, which makes achieving a good fit at early time difficult. Following Wheeler et al. (2015), we use the observed rise time t_r and photospheric velocity v_{ph} to estimate an ejecta mass M_{ej} using the equation $M_{ej} \approx 1/2 \cdot \beta \cdot c/\kappa \cdot v_{ph} t_r^2$ (Arnett 1982), where $\beta = 13.8$ is constant, c is the speed of light, t_r is the rise time, and κ is the opacity. To approximate the rise time we adopt the midpoint between the last non-detection and the first detection as the explosion epoch (MJD 60284.3, 0.9 days before detection) and the g -band peak for the time of maximum, this gives a rise time (t_r) estimate of ~ 2.75 days. For the photospheric velocity v_{ph} we use the velocity derived from spectral modelling in Section 4. Following this analysis we estimate an ejected mass $M_{ej} \sim 0.07 M_\odot$. Considering a ± 1 day uncertainty on the rise time our mass estimate could vary by $+0.06$ or $-0.04 M_\odot$. To capture the constraint in our priors we adopt a Gaussian prior on the ejecta mass M_{ej} described by $\sigma = 0.07$ and $\mu = 0.06$ on the ejected mass M_{ej} parameter.

3.3.1. Nickel Powered Explosion

We attempt to fit the multiband light curves with ^{56}Ni decay, using the built-in `default MOSFiT` model (Nadyozhin 1994; Guillochon et al. 2018). Despite a reasonable agreement with i -band observations, overall this model does not provide a satisfactory fit to the light curves of SN 2023zaw. During the SN rise the model conflicts with the deep ATLAS o -band limits, and fails to reproduce the maximum luminosity in the gcr -bands. The model clearly diverges from the late-time rz -band tail and only adequately matches the decline between MJD 60300 and MJD 60320. We find the most probable model ejects $M_{ej} = 0.06_{-0.01}^{+0.01} M_\odot$ of material with a large ^{56}Ni fraction $f_{Ni} = 0.90_{-0.11}^{+0.06}$ and a reasonable SN-like ejecta velocity $v_{ej} = 6400_{-300}^{+300} \text{ km s}^{-1}$. This implies $M_{Ni} \sim 0.05 M_\odot$ was synthesised in the explosion, this is significantly less than a typical Type Ib SN (Anderson 2019; Rodríguez et al. 2023), and is comparable to the total ejected mass. This presents a major problem for this model, contradicting our observed spectra. An ejecta of mostly ^{56}Ni and its decay products should be dominated by iron-group absorption in the blue this is not observed in the spectra of SN 2023zaw. Additionally, a nickel yield of $M_{Ni} = 0.05 M_\odot$ was difficult to rationalise in the context of the ultra-stripped SN iPTF 14gqr (Sawada et al. 2022). Clearly, a ^{56}Ni -only model does not reproduce our observations, requires an

unrealistic nickel-fraction, and can only adequately explain the light curve tail. Therefore, we exclude the scenario where nickel-decay is the only mechanism powering SN 2023zaw and seek an explanation with another mechanism in addition to nickel decay.

The light curve tail begins approximately ten days after maximum. The decline-rate slows and follows a power-law decline, an evolution which is similar to the i -band tail of the fast-fading SN 2019bkc (Chen et al. 2020; Prentice et al. 2020) where this was attributed to radioactivity.

Assuming the heating at late times is powered by decay of ^{56}Co to ^{56}Fe , we can estimate a synthesised nickel mass for SN 2023zaw. We apply the same model as before but with a restriction to fit only the late time riz -band data (MJD > 60300). The sampler only evaluates against the late-time photometry, but we provide a prior constraining the explosion epoch between the last ATLAS non-detection (MJD 60282.51) and the first detection (MJD = 60285.23). The tail requires that $M_{Ni} \sim 0.006 M_\odot$ was synthesised and ejected to power this phase of the light curve. Seeking to verify our method, we reanalyse the tail of SN 2019bkc and find a nickel mass $M_{Ni} \sim 0.005 M_\odot$, which is compatible with $M_{Ni} = 0.001 - 0.01 M_\odot$ estimated by Chen et al. (2020).

Motivated by the poor agreement of the nickel decay model to the initial peak but apparent agreement to the light curve tail, we consider a generalised early-time heating source plus a nickel decay tail. Using `MOSFiT` we adopt a physics-agnostic analytical prescription for an exponentially rising additional energy source that declines from its maximum (t_{peak}) following a power-law (named `exppow`). It is described by $L = L_{scale} \cdot (1 - e^{-t/t_{peak}})^\alpha \cdot (t/t_{peak})^{-\beta}$, where L_{scale} , α , β , and t_{peak} are free parameters. Combining the `default` and `exppow` models we created a new `MOSFiT` model called `exppowni`.

We fit the `exppowni` model as before using the same constraints on opacity and host galaxy extinction. The model realisations are shown in Figure 3. We see good agreement with observations and consistency with the ATLAS non-detections, the observed color, and late-time luminosities. We estimate a nickel mass of $M_{Ni} \sim 0.006 M_\odot$, which is in agreement with the fit for only the light curve tail. It is clear that an additional luminosity source is required to simultaneously match the fast rise, the peak luminosity and the observed ^{56}Co tail. The parameterised nature of the `exppowni` model provides insight into the timescale of the additional luminosity source, which reaches t_{peak} between 1.6 – 2.6 days after explosion and dominates the luminosity during this phase with a scale luminosity $L_{scale} \sim 10^{42} \text{ ergs s}^{-1}$.

3.3.2. Circumstellar Material Interaction + Nickel

We evaluate interaction with nearby circumstellar material (CSM) as a possible extra energy source for SN 2023zaw. CSM interaction can produce unusual and rapidly evolving transients (e.g. Moore et al. 2023; Kuncarayakti et al. 2023; Nagao et al. 2023; Perley et al. 2022). We use the CSMNI model in MOSFiT (Villar et al. 2017; Jiang et al. 2020; Moore et al. 2023) which combines the luminosity of ^{56}Ni decay and heating from shock propagation following an ejecta-CSM collision. The CSM interaction physics is implemented following the treatment of Chatzopoulos et al. (2013). We use the adapted model setup used by Moore et al. (2023) and Srivastav et al. (2023) where the onset of interaction is delayed until the ejected material reaches an inner CSM radius.

We evaluate the csmni model against our observations and show the CSM model realisations in Figure 3. This model fits the light curve peak very well and matches the overall light curve evolution in all bands, including close agreement to the late-time tail. The derived model parameters are: $M_{\text{ej}} = 0.069_{-0.004}^{+0.005} M_{\odot}$, $f_{\text{Ni}} = 0.12_{-0.02}^{+0.02}$, $r_{\text{csm}} = 63_{-12}^{+13}$ AU, $M_{\text{csm}} = 0.23_{-0.05}^{+0.06} M_{\odot}$, where, M_{csm} is the mass of the CSM material and r_{csm} is the CSM radius. This model implies $M_{\text{Ni}} \sim 0.008 M_{\odot}$, which is compatible with our estimate from just the lightcurve tail. The posterior of the CSM density profile reveals the model is insensitive to a wind or disc-like CSM structure parameter s and the CSM mass and radius show strong degeneracy. The derived kinetic energy for this model is low at $E_k \sim 10^{49}$ erg. We note the +61 day spectrum of SN 2023zaw (Das et al. 2024) shows narrow helium lines, likely from interaction. These results suggest late-stage mass loss before explosion consistent with Wu & Fuller (2022).

3.3.3. Magnetar + Nickel

We investigate the feasibility of magnetar heating as the additional energy source using the Magnetar + Nickel (‘*magni*’) model described by Nicholl et al. (2017); Gomez et al. (2022), which combines the luminosity of magnetar spin-down (Kasen & Bildsten 2010; Woosley 2010) and radioactive heating. This model is significantly better than radioactive heating alone, and matches the peak but diverges from the *riz*-band tail. Our derived Magnetar + Ni model has the following parameters, ejecta mass $M_{\text{ej}} = 0.055_{-0.005}^{+0.006} M_{\odot}$, nickel fraction $f_{\text{Ni}} = 0.08_{-0.09}^{+0.06}$, and $M_{\text{Ni}} \sim 0.004 M_{\odot}$. We find magnetar parameters of $P_{\text{spin}} = 6.3_{-1.1}^{+1.6}$ ms and $B_{\perp} = 0.19_{-0.20}^{+0.17} \times 10^{14}$ G. The B-field required from our models is consistent with the population of superluminous supernovae. However the spin period, P_{spin}

is towards the longer end of the range of 1-6 ms (e.g. Kashiyama et al. 2016; Nicholl et al. 2017). Given the low ejecta mass the region of the ejected material which is being heated by the central engine should be visible. Therefore, we would expect the W-shaped O II absorption lines to be present in the spectrum which are the characteristic signature of central engines in Type I superluminous supernovae (Mazzali et al. 2016; Quimby et al. 2018), unfortunately this region of the SN 2023zaw spectrum was not observed.

3.3.4. Shock Cooling + Nickel

Finally, we consider the contribution of ^{56}Ni and shock cooling emission of a shocked stellar envelope following the analytical Piro et al. (2021) model. In this scenario the progenitor star possesses an extended envelope which is shocked by the expanding SN and produces observable shock cooling emission. We have added this model to MOSFiT as the *pironi* model. We show our model realisations in Figure 3. Our models require $f_{\text{Ni}} = 0.01_{-0.01}^{+0.03}$, $M_{\text{ej}} = 0.04_{-0.02}^{+0.03} M_{\odot}$, $M_{\text{Ni}} \sim 0.0004 M_{\odot}$, $M_{\text{env}} \sim 0.3 M_{\odot}$, and $R_{\text{star}} = 10_{-0.4}^{+0.5} \text{ cm}$. The shock cooling model shows relatively poor agreement with the overall light curve of SN 2023zaw. The model is too luminous and contradicts the ATLAS non-detections and does not well reproduce the observed tail.

We note that this model has excellent agreement to observations when we adopt the host extinction ($A_{\text{v,host}} = 1.12$ mag) estimate made by Das et al. (2024) but not for our adopted value (see Section 3.1). Evaluating the *pironi* model with a lower value of host extinction, $A_{\text{v,host}} = 1.12$ mag, we find $f_{\text{Ni}} \sim 0.009$, an envelope mass $M_{\text{env}} \sim 0.31 M_{\odot}$, an ejected mass $M_{\text{ej}} \sim 0.03 M_{\odot}$ and a stellar radius $R_{\text{star}} \sim 10^{10.3}$ cm.

For both treatments of host extinction we find envelope masses close to or smaller than $0.2 M_{\odot}$ which is compatible with the envelope masses of an ultra-stripped progenitor (Tauris et al. 2015).

3.3.5. Model Comparison

To compare the models we use the Bayesian model evidence (marginal likelihood) scores for each model which are returned by MOSFiT when using the nested sampler Dynesty (Speagle 2020). From the Bayesian evidence scores a Bayes factor (BF) can be used to compare two models. The BF comparing model x and model y is given by $B \equiv Z_x/Z_y$, where Z_i is the Bayesian evidence for model i . A Bayes factor $B > 10$ indicates a strong preference, and $B > 100$ is considered definitive.

We find a BF $Z_{\text{expowni}}/Z_{\text{nickel}} \sim 10^{21}$, where Z_{expowni} , Z_{nickel} are the evidence for their respective models, this shows evidence favouring an additional

powering source. This statistical test and the poor agreement of ^{56}Ni only modelling with the light curves provides evidence that SN 2023zaw requires an additional power source. Comparing our Ni model and shock cooling model we find $Z_{\text{pironi}}/Z_{\text{nickel}} \sim 10^1$, the shock cooling + Ni model is preferred over Ni alone. Comparing between models in this way our analysis favours CSM + Ni model above all others. When comparing the alternative models we calculate $Z_{\text{csmni}}/Z_{\text{magni}} \sim 10^{10}$, favouring CSM interaction over the spin-down of a newly born neutron star. However, we note that the MOSFiT CSMNI model is the most complex evaluated in this work and the most flexible while likely oversimplifying the physics involved. While the CSM + Ni model reproduces the light curve tail luminosity better than any other model, the blackbody spectrum assumed in MOSFiT may be unreliable at this phase as the ejected material becomes transparent.

Through MOSFiT modelling we have shown that the total emission of SN 2023zaw cannot be explained with radioactivity alone. We have found evidence that suggests another energy source is required which peaks early in the evolution of SN 2023zaw and dominates the emission at this phase. We disfavour shock cooling emission as this additional source due to poor agreement to the multi-color photometry, in particular our ATLAS non-detections. A BF analysis favours CSM + nickel with a CSM mass which is extreme but not beyond theoretical predictions (Wu & Fuller 2022). However, a magnetar + nickel explanation for SN 2023zaw should not be ruled out. We consider both models as viable explanations for SN 2023zaw.

3.4. Spectral Modelling and Analysis

We present post-peak spectra taken +4, +8 and +26 days after maximum light. All spectra used in this work are shown in Figure 4. Our first spectrum taken +4.2 days after maximum light shows well developed absorption features and a prominent Ca II NIR triplet. Weak Fe II features may exist around 4500–5000 Å, we find that a 5700 K blackbody produces a continuum in agreement with the observed spectrum. As noted in Section 3.1 the spectra show a prominent Na I D line blend.

The spectra show little evolution between the +4 day and +8 day observations considering the rapidly evolving light curve. At +8 days the spectroscopic features have more developed line profiles and a broad emission feature at 7100 Å is apparent. Our final observation 26 days after maximum light contains little information about SN 2023zaw and we exclude it from further quantitative analysis.

SN 2023zaw was compared to a '.Ia' SN candidate SN 2010X (Karambelkar et al. 2023b), suggesting a .Ia origin for this SN. .Ia SNe are the theorised explosion of a helium shell on the surface of a white dwarf (Shen & Bildsten 2009; Shen et al. 2010). In Figure 5 we present a spectroscopic comparison to He shell detonation models (Sim et al. 2012). Although the model provides some agreement to the SED of the observed spectrum at +4.2 days, it predicts emission where in the observed spectrum we see a deep He I absorption feature at ~ 5700 Å. At +8.2 days from explosion the differences between the model and our observations become clear, the He detonation models show strong emission peaks for lines not present in data. With such clear divergence from the He detonation model we rule out a .Ia origin for SN 2023zaw, in agreement with Das et al. (2024).

Given the striking similarity to both the SEDs and spectral features of the SN 2019wxt spectra, here we undertake a similar process to that presented by Agudo et al. (2023b) of using TARDIS to model the photospheric-phase spectra. TARDIS (Kerzendorf & Sim 2014) is a one-dimensional, time-independent, Monte Carlo radiative transfer spectral synthesis code capable of simulating the spectra of an array of different explosive transients. The code assumes an inner region of completely opaque inner ejecta, beneath which all energy injection into the system is assumed to be thermalised. This inner boundary is surrounded by a number of optically thin shells that represent the line-forming region of the ejecta (these shells encompass the computational domain of the simulation). A (user-defined) number of photon quanta (dubbed r -packets) are created at the inner boundary, and are assigned properties randomly sampled from a single-temperature blackbody. The trajectory of these r -packets are simulated as they traverse the computational domain, with any interaction (either free e^- scattering, or bound-bound transitions) simulated. The r -packets that escape the outer boundary of the simulation are used to generate a synthetic spectrum, which can be compared (usually via χ -by-eye; see e.g., Stehle et al. 2005) to the observed spectrum, and iterated upon to improve agreement.

While TARDIS is a time-independent code, it is possible to evolve the input parameters to obtain a sequence of self-consistent models, as we do here for the +4.2 and +8.2 day spectra of SN 2023zaw. These user-defined input parameters include specifying the time since explosion, t_{exp} (which we set to be 2 days pre-maximum), the inner and outer boundary of the computational domain (defined in velocity-space, where $v_{\text{inner}}^{+4.2\text{d}} = 12500 \text{ km s}^{-1}$, $v_{\text{inner}}^{+8.2\text{d}} = 5000 \text{ km s}^{-1}$, and $v_{\text{outer}} = 20000 \text{ km s}^{-1}$), the

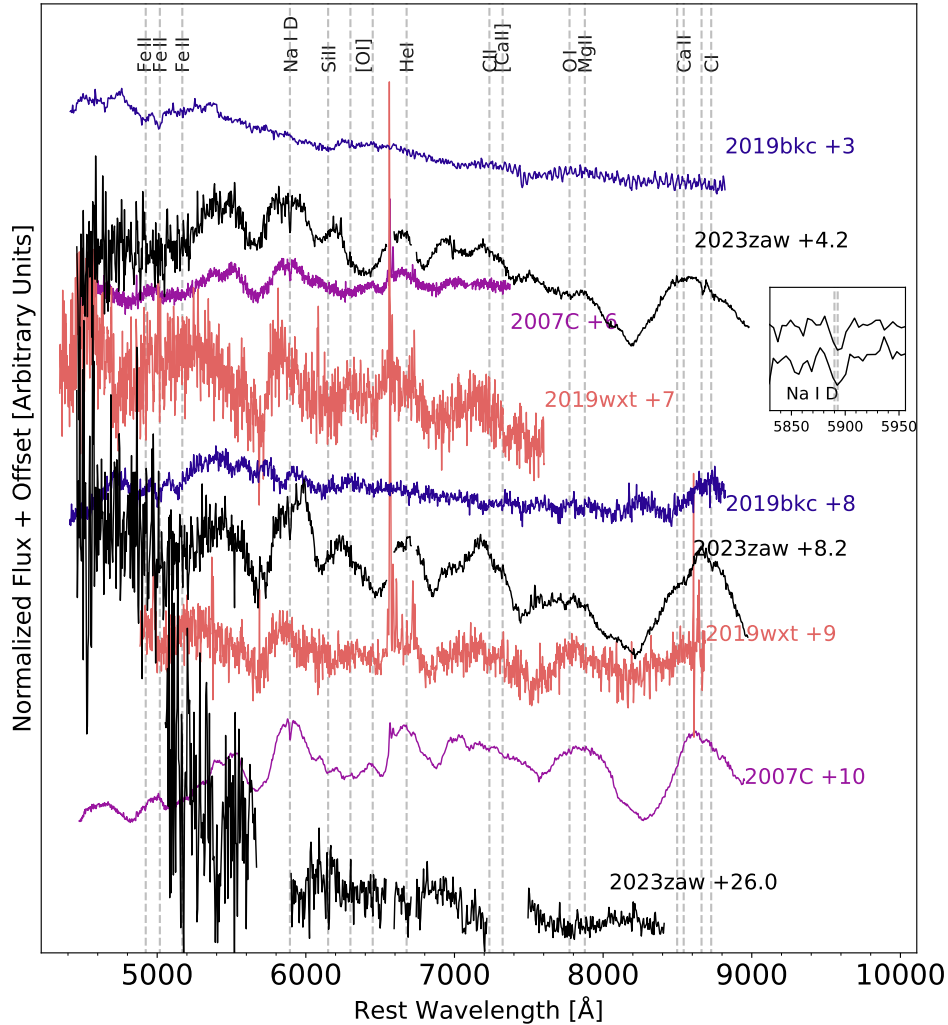


Figure 4. Optical spectroscopy of SN 2023zaw. The phase in days relative to maximum light are indicated. These spectra have been telluric and Galactic line of sight extinction corrected, and corrected for host galaxy recessional velocity. The inset plot shows the blended Na I D lines in the + 4.2 and + 8.2 day spectra. We also include spectra from SN 2019wxt (Agudo et al. 2023a), SN 2007C (Modjaz et al. 2014), SN 2019bkc (Chen et al. 2020; Prentice et al. 2020).

abundance and density of the ejecta material – here we utilise a uniform abundance across the entire ejecta and across both epochs (see Table 1), and we invoke an exponential profile, where:

$$\rho(v, t_{\text{exp}}) = 2 \times 10^{-12} \times \exp\left[\frac{-v}{6000 \text{ km s}^{-1}}\right] \times \left(\frac{2 \text{ day}}{t_{\text{exp}}}\right)^3 \text{ g cm}^{-3}. \quad (1)$$

We utilise the `dilute-lte`, `nebular` and `scatter` approximations for excitation, ionisation and line treatment, respectively, as well as including the `recomb-nlte` He treatment (as presented by Boyle et al. 2017), to better capture NLTE excitation effects for He I.

Table 1. TARDIS model compositions.

Element	Mass fraction
He	0.50
O	0.30
Si	0.20
Ca	5×10^{-6}

We present our model fits in Figure 5. The observations possess a number of prominent absorption features, located at ~ 5700 , 6100 , 6400 , 6800 , 7400 and 8200 \AA . We find that we can reproduce the +4.2 d spectrum with a relatively simple composition, made up of He, O, Si and Ca, where the 6100 \AA feature is produced by Si II, the 7400 \AA feature by O I, the 8200 \AA feature by Ca

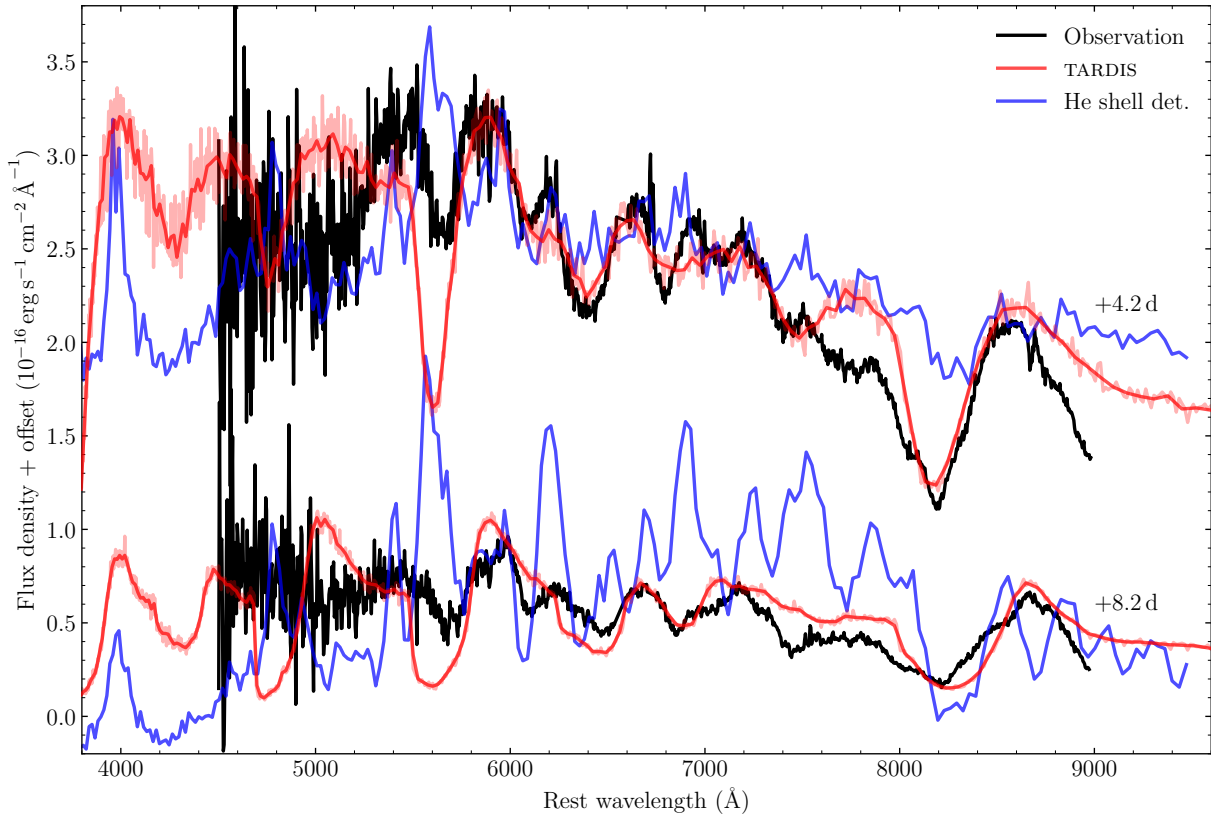


Figure 5. Best-fitting TARDIS models (red), compared to the +4.2 and +8.2 d observed spectra of SN 2023zaw (black). The +4.2 d observed spectrum (and associated model spectra) have been vertically offset for clarity (by $6 \times 10^{-17} \text{ erg s}^{-1} \text{ cm}^{-2} \text{ \AA}^{-1}$). Also plotted are two model spectra from a helium shell detonation simulation (blue) presented by Sim et al. (2012). These models have phases comparable to those of the observed spectra ($\Delta t < 0.13$ d), and have been re-scaled and arbitrarily offset to roughly match the continua of the observed spectra.

II, and all others (i.e., 5700, 6400 and 6800 \AA) by He I. We over-produce the 5700 \AA He absorption feature, and do not perfectly match the continuum blueward of $\lesssim 5400 \text{ \AA}$, but overall the fit to the data is good.

We note here that the NLTE He treatment within TARDIS is a simple, empirically-derived approximation designed to account for the effects of recombination from He II \rightarrow He I. As such, it is possible that the estimated level populations within our TARDIS simulation have deviated from the true level populations. This possible issue has been noted before, and was proposed as the reason behind the disagreement between the relative strengths of He features in the case of SN 2019wxt (Agudo et al. 2023b). There, they manually altered the relative level populations of He I to better match the observed relative strengths of the He I features. Here we opt to not explore such variations, as our focus is on constraining the elements that dominate the composition in the line-forming region of the ejecta material of SN 2023zaw.

Attempts to fit the observations in a more detailed manner than presented here should be approached with

extreme caution, given we have no reliable constraint on the true level of extinction. As a result, the true continuum of these observed spectra could be much bluer than what we present here (see Section 3.1 for details on our extinction estimates), which would significantly alter the agreement of our models to the data.

Although our model composition is quite rudimentary, it aligns with our SN Ib classification, and not .Ia. Going beyond classification arguments, we are able to constrain the composition to be $\sim 80\%$ He and O, and $\sim 20\%$ Si (in the line-forming region). Our inner velocity estimates derived from this modelling ($v_{\text{inner}}^{+4.2 \text{ d}} = 12500 \text{ km s}^{-1}$ and $v_{\text{inner}}^{+8.2 \text{ d}} = 5000 \text{ km s}^{-1}$) indicates the photosphere is receding quickly into the ejecta material, consistent with a small mass of ejected material.

3.5. Volumetric Rates

Here we present a preliminary volumetric rate estimate for SN 2023zaw-like rapidly evolving stripped-envelope SNe (SESNe). We use the methodology described by Srivastav et al. (2022) for estimating rates of

SNe Iax. We consider rapidly evolving SESNe detected by the ATLAS survey that occurred within a distance of 100 Mpc during a 5 year window spanning 2017 September 21 and 2022 September 20 (Srivastav et al. 2022). To estimate the recovery efficiency of SN 2023zaw-like transients within 100 Mpc, we use the ATLAS survey simulator (McBrien 2021). We use Gaussian Processes interpolated ATLAS *c* and *o*-band light curves of SN 2023zaw, produced by interpolating the light curves using the public `extraboi` (Thornton et al. 2023) code. These were then injected 10,000 times at a range of times, sky locations and redshift bins spanning up to $D = 100$ Mpc in the simulation. A simulated transient was considered to be recovered as a detection if it produced a minimum of 6 to 8 detections of 5σ (or greater) significance. Although difference detections in the ATLAS data stream are flagged as candidate transients if they produce 3 individual 5σ detections on any given night, this criterion is more realistic since human scanners will be confident about promoting candidates to the TNS if they have detections over at least two distinct nights.

The volumetric rate is thus estimated using

$$R = \frac{N}{\eta VT},$$

where T is the time duration of the mock survey, N is the number of ultra-stripped SNe detected within the considered time duration, η represents the recovery efficiency from the ATLAS survey simulator and V is the volume probed within 100 Mpc. We consider $N = 3$, representing SN 2019bkc (Prentice et al. 2020; Chen et al. 2020), SN 2019dge (Yao et al. 2020) and SN 2021agco (Yan et al. 2023). The recovery efficiency obtained from the survey simulator is $\eta \approx 0.06 \pm 0.02$.

From the above, we estimate a rate of $R \approx 2.5_{-1.4}^{+2.5} \pm 0.9 \times 10^{-6} \text{ Mpc}^{-3} \text{ yr}^{-1} h_{70}^3$ for rapidly evolving SN 2023zaw-like SESNe, where $h_{70} = H_0/70$. The statistical uncertainty derives from 1σ Gaussian errors from single-sided upper and lower limits for Poisson statistics (Gehrels 1986) and the systematic uncertainty is based on the error on the recovery efficiency η . The above rate estimate for SN 2023zaw-like SESNe accounts for $\sim 1 - 6\%$ of the CCSN rate and $\sim 5 - 20\%$ of the SESN rate computed by Frohmaier et al. (2021). We note here that $\sim 15\%$ of transients in the 100 Mpc ATLAS sample do not have a spectroscopic classification (Srivastav et al. 2022), and it is possible that the representation of SN 2023zaw-like rapidly evolving SESNe is disproportionately higher within the unclassified sample. Nonetheless, at a few per cent of the CCSN rate, these transients clearly constitute a rare class of stellar explosions.

3.6. Potential Evolutionary Route

Using the physical characteristics inferred from our analysis we can look for potential progenitor systems in the Binary Population and Spectral Synthesis data release (BPASSv2.2.2 Eldridge et al. 2017; Stanway & Eldridge 2018; Stevance et al. 2020). Assuming a solar metallicity ($Z=0.02$) we look for models with $M_H < 0.01 M_\odot$ and hydrogen mass fraction $X < 0.001$ (Dessart et al. 2012). An inferred low ejecta mass in Section 3.3 further constrains our search to models with ejecta mass $< 0.1 M_\odot$. Given the low kinetic energy and ejecta mass of SN 2023zaw we report below the results obtained by assuming the lower supernova explosion energy (10^{50} ergs). In addition we apply a condition for explodability of the progenitor star, commonly a threshold on the mass of the Oxygen Neon core ($>1.38 M_\odot$) is used to determine if a model is a candidate for core collapse. When this condition is applied no models in BPASSv2.2.2 are found to match all of our conditions; but relaxing the condition to an ONe core mass greater than $1.30 M_\odot$ (removing one significant figure from the threshold), we find 10 models that fit our criteria. When we include weights dependent on the Initial Mass Function as well as the binary fractions and period distributions (our fiducial IMF – Kroupa 2001 – and our binary fractions and period distributions are based on Moe & Di Stefano 2017), this corresponds to 28 such systems per million solar masses at solar metallicity.

BPASS data are a grid of stellar evolution models and does not contain all possible observable outcomes. However, natively finding candidate progenitor stars just at the threshold of explodability is interesting when considering the observed rarity of SN 2023zaw-like explosions. The progenitor of SN 2023zaw is very likely a lower mass star: the initial masses of our 6 systems on the cusp of explodability range from 7.5 to $9 M_\odot$, which due to the initial mass function are some of the most common massive stars in the Universe. The low rate of SN 2023zaw-like SNe and BPASS results are naturally reconciled if potential progenitors of these SNe fail to explode most of the time, as their cores do not reach the necessary physical conditions. The 10 models we find with ONe core mass $> 1.3 M_\odot$ represent only 2.6 percent of the massive stars ($M_{ZAMS} > 7.5 M_\odot$) that fit our stripping and ejecta mass criteria, and it is unlikely all of these would explode. This is in agreement with the calculated rates in Section 3.5 of a few percent of the CCSN rate.

4. SUMMARY AND CONCLUSIONS

In this section we summarize the properties of SN 2023zaw.

1. SN 2023zaw shows a rapid rise (< 4 rest-frame days), and initial decline from maximum light which settles to a radioactive tail 10 days after peak. Comparisons to USSNe and rapidly evolving supernovae shows that SN 2023zaw is among the fastest fading SNe yet discovered, comparable to SN 2019bkc (Chen et al. 2020; Prentice et al. 2020). We consider radioactive nickel as the power source for SN 2023zaw, finding that nickel alone cannot power both the peak and the tail of the lightcurve, unlike SN 2019dge and SN 2019wxt (Yao et al. 2020; Agudo et al. 2023a). An additional power source is required.
2. We consider several additional powering mechanisms and use a Bayes factor analysis to select a preferred model. This analysis favors interaction with a CSM ($M_{\text{CSM}} = 0.23_{-0.05}^{+0.06} M_{\odot}$ $r_{\text{CSM}} = 63_{-12}^{+13}$ AU) to boost the initial luminosity of SN 2023zaw. We note that spectroscopic signatures of interaction were not observed in the spectra and suggest that the CSM envelope was swept up by the photosphere before our first spectroscopic observation.
3. Through spectroscopic comparison we show SN 2023zaw is similar to type Ib SNe and shows lines and line strengths similar to SN 2007C (Modjaz et al. 2014) and SN 2019wxt (Agudo et al. 2023a). Monte Carlo radiative transfer modelling with TARDIS shows SN 2023zaw has a composition dominated by He, O and Si. The spectroscopic evolution is not compatible with He shell detonation models.
4. A simulated ATLAS survey and estimate of the spectroscopic completeness of the ATLAS Volume Limited Survey ($D < 100$ Mpc) yields a rates estimate of $R \approx 2.5_{-1.4}^{+2.5} \pm 0.9 \times 10^{-6} \text{ Mpc}^{-3} \text{ yr}^{-1} h_{70}^3$. SN 2023zaw-like transients could be as common as $\sim 1 - 6\%$ of the CCSN rate. Searching for potential progenitor stars in BPASS models we propose that SN 2023zaw-like events are the result of lower mass progenitors ($M_{\text{ZAMS}} = 7.5 - 9 M_{\odot}$) whose cores are at the threshold of explodability. The low observed rate of these SNe is then a result of the fact that only a few percent of these stars end with a core mass sufficient to result in core collapse.

We have shown SN 2023zaw to be part of a small group of rapidly evolving SNe with a low ejecta mass ($M \simeq 0.07 M_{\odot}$) and estimated a total nickel mass synthesised in the explosion $M_{\text{Ni}} \simeq 0.006 M_{\odot}$. Furthermore, through BF analysis we find evidence in favour of an extra luminosity source in addition to the radioactive

decay of ^{56}Ni . With our estimate of host galaxy extinction and significant Milky Way extinction in the line of sight we cannot reproduce the observe light curve with shock cooling emission as favoured by (Das et al. 2024) and favour interaction with a detached CSM to boost the luminosity of SN 2023zaw or magnetar energy injection.

ACKNOWLEDGMENTS

SJS, SS, KWS and DRY acknowledge funding from STFC Grants ST/Y001605/1, ST/X001253/1, ST/X006506/1 and ST/T000198/1. SJS acknowledges a Royal Society Research Professorship. MN is supported by the European Research Council (ERC) under the European Union’s Horizon 2020 research and innovation programme (grant agreement No. 948381) and by UK Space Agency Grant No. ST/Y000692/1. TWC acknowledges the Yushan Young Fellow Program by the Ministry of Education, Taiwan for the financial support. SY acknowledges the funding from the National Natural Science Foundation of China under Grant No. 12303046. HFS is supported by the Eric and Wendy Schmidt A.I. in Science Fellowship. Pan-STARRS is primarily funded to search for near-earth asteroids through NASA grants NNX08AR22G and NNX14AM74G. The Pan-STARRS science products for transient follow-up are made possible through the contributions of the University of Hawaii Institute for Astronomy and Queen’s University Belfast. ATLAS is primarily funded through NASA grants NN12AR55G, 80NSSC18K0284, and 80NSSC18K1575. The ATLAS science products are provided by the University of Hawaii, Queen’s University Belfast, STScI, SAAO and Millennium Institute of Astrophysics in Chile. We thank Lulin staff H.-Y. Hsiao, W.-J. Hou, C.-S. Lin, H.-C. Lin, and J.-K. Guo for observations and data management. Based on observations obtained at the international Gemini Observatory (under program ID GN-2023B-Q-125), a program of NSF NOIRLab, which is managed by the Association of Universities for Research in Astronomy (AURA) under a cooperative agreement with the U.S. National Science Foundation on behalf of the Gemini Observatory partnership: the U.S. National Science Foundation (United States), National Research Council (Canada), Agencia Nacional de Investigación y Desarrollo (Chile), Ministerio de Ciencia, Tecnología e Innovación (Argentina), Ministério da Ciência, Tecnologia, Inovações e Comunicações (Brazil), and Korea Astronomy and Space Science Institute (Republic of Korea). This work was enabled by observations made from the Gemini North telescope, located within the Maunakea Science Reserve and adjacent to the summit of

Maunakea. We are grateful for the privilege of observing the Universe from a place that is unique in both its astronomical quality and its cultural significance. Lairsair is supported by the UKRI Science and Technology Facilities Council and is a collaboration between the University of Edinburgh (grant ST/N002512/1) and QUB (grant ST/N002520/1) within the LSST:UK Science Consortium. ZTF is supported by National Science Foundation grant AST-1440341 and a collaboration including Caltech, IPAC, the Weizmann Institute for Science, the Oskar Klein Center at Stockholm University, the University of Maryland, the University of Washington, Deutsches Elektronen-Synchrotron and Hum-

boldt University, Los Alamos National Laboratories, the TANGO Consortium of Taiwan, the University of Wisconsin at Milwaukee, and Lawrence Berkeley National Laboratories.

Facilities: Gemini:Gillett, Swift, PS1, PO:1.2m, Liverpool:2m

Software: Astropy (Astropy Collaboration et al. 2013, 2018, 2022), Numpy (Harris et al. 2020), Matplotlib (Hunter 2007), Mosfit (Guillochon et al. 2018), Hoki (Stevance et al. 2020), PSF (Nicholl et al. 2023), DRAGONS (Labrie et al. 2023; Labrie et al. 2023)

APPENDIX

A. MOSFIT MODEL POSTERIOR

REFERENCES

- Agudo, I., Amati, L., An, T., et al. 2023a, *A&A*, 675, A201, doi: [10.1051/0004-6361/202244751](https://doi.org/10.1051/0004-6361/202244751)
- . 2023b, *A&A*, 675, A201, doi: [10.1051/0004-6361/202244751](https://doi.org/10.1051/0004-6361/202244751)
- Anderson, J. P. 2019, *A&A*, 628, A7, doi: [10.1051/0004-6361/201935027](https://doi.org/10.1051/0004-6361/201935027)
- Arnett, W. D. 1982, *ApJ*, 253, 785, doi: [10.1086/159681](https://doi.org/10.1086/159681)
- Astropy Collaboration, Robitaille, T. P., Tollerud, E. J., et al. 2013, *A&A*, 558, A33, doi: [10.1051/0004-6361/201322068](https://doi.org/10.1051/0004-6361/201322068)
- Astropy Collaboration, Price-Whelan, A. M., Sipőcz, B. M., et al. 2018, *AJ*, 156, 123, doi: [10.3847/1538-3881/aabc4f](https://doi.org/10.3847/1538-3881/aabc4f)
- Astropy Collaboration, Price-Whelan, A. M., Lim, P. L., et al. 2022, *ApJ*, 935, 167, doi: [10.3847/1538-4357/ac7c74](https://doi.org/10.3847/1538-4357/ac7c74)
- Bellm, E. C., Kulkarni, S. R., Graham, M. J., et al. 2019, *PASP*, 131, 018002, doi: [10.1088/1538-3873/aaecbe](https://doi.org/10.1088/1538-3873/aaecbe)
- Bertin, E., & Arnouts, S. 1996, *A&AS*, 117, 393, doi: [10.1051/aas:1996164](https://doi.org/10.1051/aas:1996164)
- Boyle, A., Sim, S. A., Hachinger, S., & Kerzendorf, W. 2017, *A&A*, 599, A46, doi: [10.1051/0004-6361/201629712](https://doi.org/10.1051/0004-6361/201629712)
- Breeveld, A. A., Landsman, W., Holland, S. T., et al. 2011, in *American Institute of Physics Conference Series*, Vol. 1358, American Institute of Physics Conference Series, ed. J. E. McEnery, J. L. Racusin, & N. Gehrels, 373–376, doi: [10.1063/1.3621807](https://doi.org/10.1063/1.3621807)
- Chambers, K. C., Magnier, E. A., Metcalfe, N., et al. 2016, *ArXiv e-prints*. <https://arxiv.org/abs/1612.05560>
- Chatzopoulos, E., Wheeler, J. C., Vinko, J., Horvath, Z. L., & Nagy, A. 2013, *ApJ*, 773, 76, doi: [10.1088/0004-637X/773/1/76](https://doi.org/10.1088/0004-637X/773/1/76)
- Chen, P., Dong, S., Stritzinger, M. D., et al. 2020, *ApJL*, 889, L6, doi: [10.3847/2041-8213/ab62a4](https://doi.org/10.3847/2041-8213/ab62a4)
- Chen, T. W., Yang, S., Pan, Y. C., et al. 2021, *Transient Name Server AstroNote*, 92, 1
- Das, K. K., Fremling, C., Kasliwal, M. M., et al. 2024, *arXiv e-prints*, arXiv:2403.08165, doi: [10.48550/arXiv.2403.08165](https://doi.org/10.48550/arXiv.2403.08165)
- De, K., Kasliwal, M. M., Ofek, E. O., et al. 2018, *Science*, 362, 201, doi: [10.1126/science.aas8693](https://doi.org/10.1126/science.aas8693)
- Dessart, L., Hillier, D. J., Li, C., & Woosley, S. 2012, *MNRAS*, 424, 2139, doi: [10.1111/j.1365-2966.2012.21374.x](https://doi.org/10.1111/j.1365-2966.2012.21374.x)
- Drout, M. R., Soderberg, A. M., Gal-Yam, A., et al. 2011, *ApJ*, 741, 97, doi: [10.1088/0004-637X/741/2/97](https://doi.org/10.1088/0004-637X/741/2/97)
- Drout, M. R., Soderberg, A. M., Mazzali, P. A., et al. 2013, *ApJ*, 774, 58, doi: [10.1088/0004-637X/774/1/58](https://doi.org/10.1088/0004-637X/774/1/58)
- Eldridge, J. J., Stanway, E. R., Xiao, L., et al. 2017, *PASA*, 34, e058, doi: [10.1017/pasa.2017.51](https://doi.org/10.1017/pasa.2017.51)
- Frohmaier, C., Angus, C. R., Vincenzi, M., et al. 2021, *MNRAS*, 500, 5142, doi: [10.1093/mnras/staa3607](https://doi.org/10.1093/mnras/staa3607)
- Fulton, M., Moore, T., Srivastav, S., et al. 2023, *Transient Name Server AstroNote*, 339, 1
- Gehrels, N. 1986, *ApJ*, 303, 336, doi: [10.1086/164079](https://doi.org/10.1086/164079)
- Gehrels, N., Chincarini, G., Giommi, P., et al. 2004, *ApJ*, 611, 1005, doi: [10.1086/422091](https://doi.org/10.1086/422091)
- Gillanders, J. H., Sim, S. A., & Smartt, S. J. 2020, *MNRAS*, 497, 246, doi: [10.1093/mnras/staa1822](https://doi.org/10.1093/mnras/staa1822)
- Gillanders, J. H., Huber, M., Chambers, K., et al. 2023, *Transient Name Server AstroNote*, 341, 1

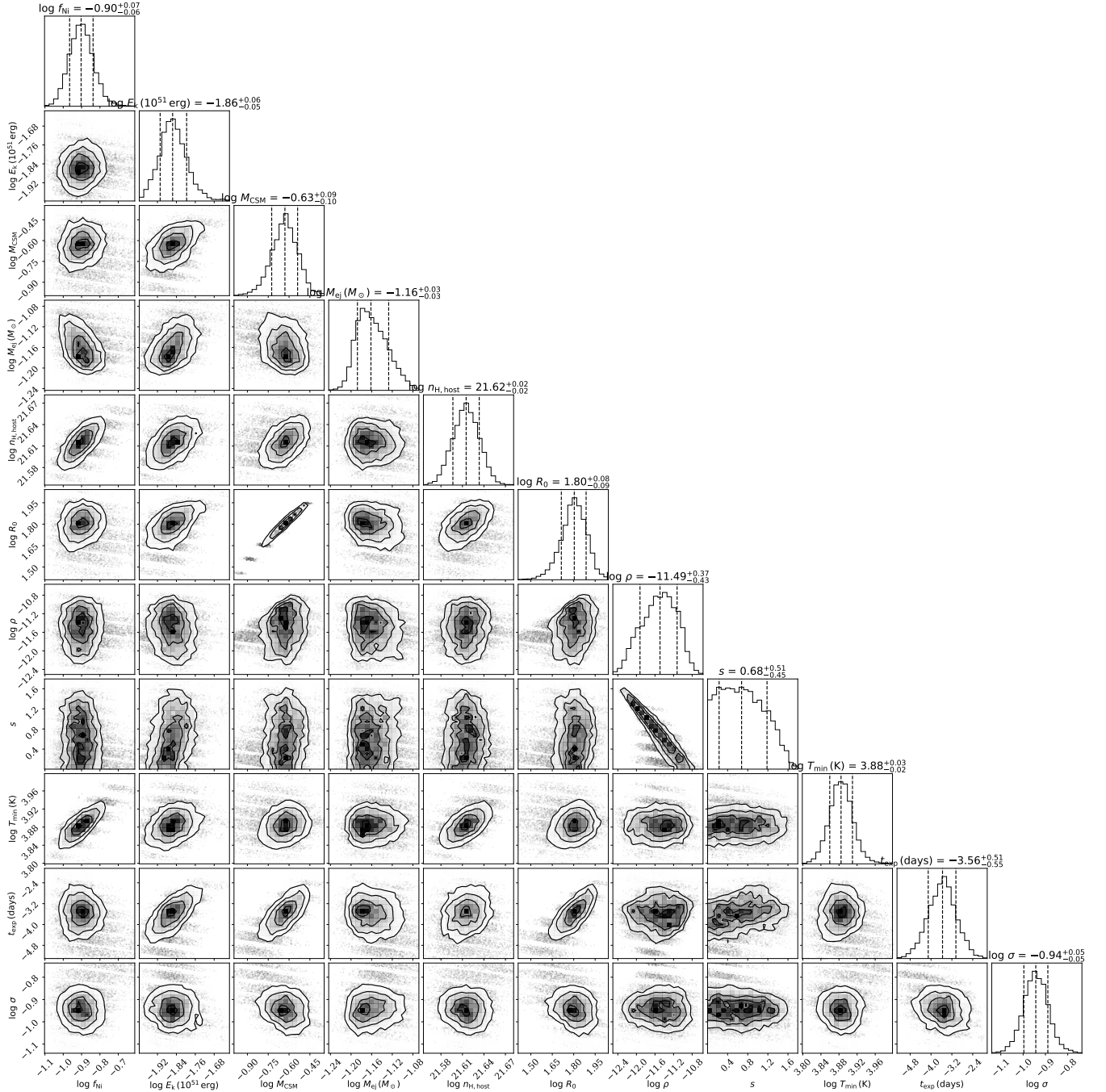


Figure 6. Physical parameter posterior distribution of the circumstellar material + nickel model. Where the important physical parameters are nickel fraction (f_{Ni}), kinetic energy (E_k), CSM mass (M_{CSM}), ejecta mass (M_{ej}), the CSM radius (R_0) in units of AU, CSM density (ρ), t_{exp} is relative to the first photometric detection (MJD 60285.23) of SN 2023zaw.

Gomez, S., Berger, E., Nicholl, M., Blanchard, P. K., & Hosseinzadeh, G. 2022, ApJ, 941, 107, doi: [10.3847/1538-4357/ac9842](https://doi.org/10.3847/1538-4357/ac9842)

Guillochon, J., Nicholl, M., Villar, V. A., et al. 2018, ApJS, 236, 6, doi: [10.3847/1538-4365/aab761](https://doi.org/10.3847/1538-4365/aab761)

Güver, T., & Özel, F. 2009, MNRAS, 400, 2050, doi: [10.1111/j.1365-2966.2009.15598.x](https://doi.org/10.1111/j.1365-2966.2009.15598.x)

Harris, C. R., Millman, K. J., van der Walt, S. J., et al. 2020, Nature, 585, 357, doi: [10.1038/s41586-020-2649-2](https://doi.org/10.1038/s41586-020-2649-2)

Ho, A. Y. Q., Perley, D. A., Gal-Yam, A., et al. 2023, ApJ, 949, 120, doi: [10.3847/1538-4357/acc533](https://doi.org/10.3847/1538-4357/acc533)

Hunter, J. D. 2007, Computing in Science & Engineering, 9, 90, doi: [10.1109/MCSE.2007.55](https://doi.org/10.1109/MCSE.2007.55)

- Insera, C. 2019, *Nature Astronomy*, 3, 697, doi: [10.1038/s41550-019-0854-4](https://doi.org/10.1038/s41550-019-0854-4)
- Jiang, B., Jiang, S., & Ashley Villar, V. 2020, *Research Notes of the American Astronomical Society*, 4, 16, doi: [10.3847/2515-5172/ab7128](https://doi.org/10.3847/2515-5172/ab7128)
- Karambelkar, V., Andreoni, I., Sollerman, J., et al. 2023a, *Transient Name Server AstroNote*, 335, 1
- Karambelkar, V., Das, K., Lin, Z., et al. 2023b, *Transient Name Server AstroNote*, 340, 1
- Kasen, D., & Bildsten, L. 2010, *ApJ*, 717, 245, doi: [10.1088/0004-637X/717/1/245](https://doi.org/10.1088/0004-637X/717/1/245)
- Kashiyama, K., Murase, K., Bartos, I., Kiuchi, K., & Margutti, R. 2016, *ApJ*, 818, 94, doi: [10.3847/0004-637X/818/1/94](https://doi.org/10.3847/0004-637X/818/1/94)
- Kasliwal, M. M., Kulkarni, S. R., Gal-Yam, A., et al. 2010, *ApJL*, 723, L98, doi: [10.1088/2041-8205/723/1/L98](https://doi.org/10.1088/2041-8205/723/1/L98)
- Kerzendorf, W. E., & Sim, S. A. 2014, *MNRAS*, 440, 387, doi: [10.1093/mnras/stu055](https://doi.org/10.1093/mnras/stu055)
- Kroupa, P. 2001, *MNRAS*, 322, 231, doi: [10.1046/j.1365-8711.2001.04022.x](https://doi.org/10.1046/j.1365-8711.2001.04022.x)
- Kuncarayakti, H., Sollerman, J., Izzo, L., et al. 2023, *arXiv e-prints*, arXiv:2303.16925, doi: [10.48550/arXiv.2303.16925](https://doi.org/10.48550/arXiv.2303.16925)
- Labrie, K., Simpson, C., Cardenas, R., et al. 2023, *Research Notes of the American Astronomical Society*, 7, 214, doi: [10.3847/2515-5172/ad0044](https://doi.org/10.3847/2515-5172/ad0044)
- Labrie, K., Simpson, C., Turner, J., et al. 2023, *DRAGONS*, 3.1.0, Zenodo, doi: [10.5281/zenodo.7776065](https://doi.org/10.5281/zenodo.7776065)
- Lee, M. H., Zeng, K. J., Chen, T. W., et al. 2023, *Transient Name Server AstroNote*, 338, 1
- Mazzali, P. A., Sullivan, M., Pian, E., Greiner, J., & Kann, D. A. 2016, *MNRAS*, 458, 3455, doi: [10.1093/mnras/stw512](https://doi.org/10.1093/mnras/stw512)
- McBrien, O. 2021, PhD thesis, Queen's University Belfast
- Modjaz, M., Gutiérrez, C. P., & Arcavi, I. 2019, *Nature Astronomy*, 3, 717, doi: [10.1038/s41550-019-0856-2](https://doi.org/10.1038/s41550-019-0856-2)
- Modjaz, M., Blondin, S., Kirshner, R. P., et al. 2014, *AJ*, 147, 99, doi: [10.1088/0004-6256/147/5/99](https://doi.org/10.1088/0004-6256/147/5/99)
- Moe, M., & Di Stefano, R. 2017, *ApJS*, 230, 15, doi: [10.3847/1538-4365/aa6fb6](https://doi.org/10.3847/1538-4365/aa6fb6)
- Moore, T., Smartt, S. J., Nicholl, M., et al. 2023, *ApJL*, 956, L31, doi: [10.3847/2041-8213/acfc25](https://doi.org/10.3847/2041-8213/acfc25)
- Moriya, T. J., Mazzali, P. A., Tominaga, N., et al. 2017, *MNRAS*, 466, 2085, doi: [10.1093/mnras/stw3225](https://doi.org/10.1093/mnras/stw3225)
- Nadyozhin, D. K. 1994, *ApJS*, 92, 527, doi: [10.1086/192008](https://doi.org/10.1086/192008)
- Nagao, T., Kuncarayakti, H., Maeda, K., et al. 2023, *A&A*, 673, A27, doi: [10.1051/0004-6361/202346084](https://doi.org/10.1051/0004-6361/202346084)
- Nicholl, M., Guillochon, J., & Berger, E. 2017, *ApJ*, 850, 55, doi: [10.3847/1538-4357/aa9334](https://doi.org/10.3847/1538-4357/aa9334)
- Nicholl, M., Srivastav, S., Fulton, M. D., et al. 2023, *ApJL*, 954, L28, doi: [10.3847/2041-8213/acf0ba](https://doi.org/10.3847/2041-8213/acf0ba)
- Perley, D., Sollerman, J., Schulze, S., et al. 2022, in *American Astronomical Society Meeting Abstracts*, Vol. 54, American Astronomical Society Meeting #240, 232.08
- Piro, A. L., Haynie, A., & Yao, Y. 2021, *ApJ*, 909, 209, doi: [10.3847/1538-4357/abe2b1](https://doi.org/10.3847/1538-4357/abe2b1)
- Poole, T. S., Breeveld, A. A., Page, M. J., et al. 2008, 383, 627, doi: [10.1111/j.1365-2966.2007.12563.x](https://doi.org/10.1111/j.1365-2966.2007.12563.x)
- Poznanski, D., Prochaska, J. X., & Bloom, J. S. 2012, *MNRAS*, 426, 1465, doi: [10.1111/j.1365-2966.2012.21796.x](https://doi.org/10.1111/j.1365-2966.2012.21796.x)
- Poznanski, D., Chornock, R., Nugent, P. E., et al. 2010, *Science*, 327, 58, doi: [10.1126/science.1181709](https://doi.org/10.1126/science.1181709)
- Prentice, S. J., Maguire, K., Smartt, S. J., et al. 2018, *ApJL*, 865, L3, doi: [10.3847/2041-8213/aadd90](https://doi.org/10.3847/2041-8213/aadd90)
- Prentice, S. J., Maguire, K., Flörs, A., et al. 2020, *A&A*, 635, A186, doi: [10.1051/0004-6361/201936515](https://doi.org/10.1051/0004-6361/201936515)
- Quimby, R. M., De Cia, A., Gal-Yam, A., et al. 2018, *ApJ*, 855, 2, doi: [10.3847/1538-4357/aaac2f](https://doi.org/10.3847/1538-4357/aaac2f)
- Rodríguez, Ó., Maoz, D., & Nakar, E. 2023, *ApJ*, 955, 71, doi: [10.3847/1538-4357/ace2bd](https://doi.org/10.3847/1538-4357/ace2bd)
- Roming, P. W. A., Kennedy, T. E., Mason, K. O., et al. 2005, *SSRv*, 120, 95, doi: [10.1007/s11214-005-5095-4](https://doi.org/10.1007/s11214-005-5095-4)
- Sawada, R., Kashiyama, K., & Suwa, Y. 2022, *ApJ*, 927, 223, doi: [10.3847/1538-4357/ac53ae](https://doi.org/10.3847/1538-4357/ac53ae)
- Schlafly, E. F., & Finkbeiner, D. P. 2011, *ApJ*, 737, 103, doi: [10.1088/0004-637X/737/2/103](https://doi.org/10.1088/0004-637X/737/2/103)
- Shen, K. J., & Bildsten, L. 2009, *ApJ*, 699, 1365, doi: [10.1088/0004-637X/699/2/1365](https://doi.org/10.1088/0004-637X/699/2/1365)
- Shen, K. J., Kasen, D., Weinberg, N. N., Bildsten, L., & Scannapieco, E. 2010, *ApJ*, 715, 767, doi: [10.1088/0004-637X/715/2/767](https://doi.org/10.1088/0004-637X/715/2/767)
- Shingles, L., Smith, K. W., Young, D. R., et al. 2021, *Transient Name Server AstroNote*, 7, 1
- Sim, S. A., Fink, M., Kromer, M., et al. 2012, *MNRAS*, 420, 3003, doi: [10.1111/j.1365-2966.2011.20162.x](https://doi.org/10.1111/j.1365-2966.2011.20162.x)
- Smith, K. W., Williams, R. D., Young, D. R., et al. 2019, *Research Notes of the American Astronomical Society*, 3, 26, doi: [10.3847/2515-5172/ab020f](https://doi.org/10.3847/2515-5172/ab020f)
- Smith, K. W., Smartt, S. J., Young, D. R., et al. 2020, *PASP*, 132, 085002, doi: [10.1088/1538-3873/ab936e](https://doi.org/10.1088/1538-3873/ab936e)
- Sollerman, J. 2023, *Transient Name Server Discovery Report*, 2023-3158, 1
- Speagle, J. S. 2020, *MNRAS*, 493, 3132, doi: [10.1093/mnras/staa278](https://doi.org/10.1093/mnras/staa278)
- Springob, C. M., Haynes, M. P., Giovanelli, R., & Kent, B. R. 2005, *ApJS*, 160, 149, doi: [10.1086/431550](https://doi.org/10.1086/431550)

- Srivastav, S., Smartt, S. J., Huber, M. E., et al. 2022, MNRAS, 511, 2708, doi: [10.1093/mnras/stac177](https://doi.org/10.1093/mnras/stac177)
- Srivastav, S., Moore, T., Nicholl, M., et al. 2023, ApJL, 956, L34, doi: [10.3847/2041-8213/acffaf](https://doi.org/10.3847/2041-8213/acffaf)
- Stanway, E. R., & Eldridge, J. J. 2018, MNRAS, 479, 75, doi: [10.1093/mnras/sty1353](https://doi.org/10.1093/mnras/sty1353)
- Steele, I. A., Smith, R. J., Rees, P. C., et al. 2004, in Society of Photo-Optical Instrumentation Engineers (SPIE) Conference Series, Vol. 5489, Ground-based Telescopes, ed. J. Oschmann, Jacobus M., 679–692, doi: [10.1117/12.551456](https://doi.org/10.1117/12.551456)
- Stehle, M., Mazzali, P. A., Benetti, S., & Hillebrandt, W. 2005, MNRAS, 360, 1231, doi: [10.1111/j.1365-2966.2005.09116.x](https://doi.org/10.1111/j.1365-2966.2005.09116.x)
- Stevance, H., Eldridge, J., & Stanway, E. 2020, The Journal of Open Source Software, 5, 1987, doi: [10.21105/joss.01987](https://doi.org/10.21105/joss.01987)
- Stritzinger, M., Mazzali, P., Phillips, M. M., et al. 2009, ApJ, 696, 713, doi: [10.1088/0004-637X/696/1/713](https://doi.org/10.1088/0004-637X/696/1/713)
- Stritzinger, M. D., Anderson, J. P., Contreras, C., et al. 2018, A&A, 609, A134, doi: [10.1051/0004-6361/201730842](https://doi.org/10.1051/0004-6361/201730842)
- Tauris, T. M., Langer, N., & Podsiadlowski, P. 2015, MNRAS, 451, 2123, doi: [10.1093/mnras/stv990](https://doi.org/10.1093/mnras/stv990)
- Thornton, I., Villar, V. A., Gomez, S., & Hosseinzadeh, G. 2023, in American Astronomical Society Meeting Abstracts, Vol. 55, American Astronomical Society Meeting Abstracts, 107.24
- Tonry, J. L., Denneau, L., Heinze, A. N., et al. 2018, PASP, 130, 064505, doi: [10.1088/1538-3873/aabadf](https://doi.org/10.1088/1538-3873/aabadf)
- Tully, R. B., Courtois, H. M., Dolphin, A. E., et al. 2013, AJ, 146, 86, doi: [10.1088/0004-6256/146/4/86](https://doi.org/10.1088/0004-6256/146/4/86)
- Villar, V. A., Berger, E., Metzger, B. D., & Guillochon, J. 2017, ApJ, 849, 70, doi: [10.3847/1538-4357/aa8fcb](https://doi.org/10.3847/1538-4357/aa8fcb)
- Wheeler, J. C., Johnson, V., & Clocchiatti, A. 2015, MNRAS, 450, 1295, doi: [10.1093/mnras/stv650](https://doi.org/10.1093/mnras/stv650)
- Woosley, S. E. 2010, ApJL, 719, L204, doi: [10.1088/2041-8205/719/2/L204](https://doi.org/10.1088/2041-8205/719/2/L204)
- Woosley, S. E., Pinto, P. A., & Hartmann, D. 1989, ApJ, 346, 395, doi: [10.1086/168019](https://doi.org/10.1086/168019)
- Wu, S. C., & Fuller, J. 2022, ApJL, 940, L27, doi: [10.3847/2041-8213/ac9b3d](https://doi.org/10.3847/2041-8213/ac9b3d)
- Yan, S., Wang, X., Gao, X., et al. 2023, ApJL, 959, L32, doi: [10.3847/2041-8213/ad0cc3](https://doi.org/10.3847/2041-8213/ad0cc3)
- Yao, Y., De, K., Kasliwal, M. M., et al. 2020, ApJ, 900, 46, doi: [10.3847/1538-4357/abaa3d](https://doi.org/10.3847/1538-4357/abaa3d)
- Yaron, O., & Gal-Yam, A. 2012, PASP, 124, 668, doi: [10.1086/666656](https://doi.org/10.1086/666656)